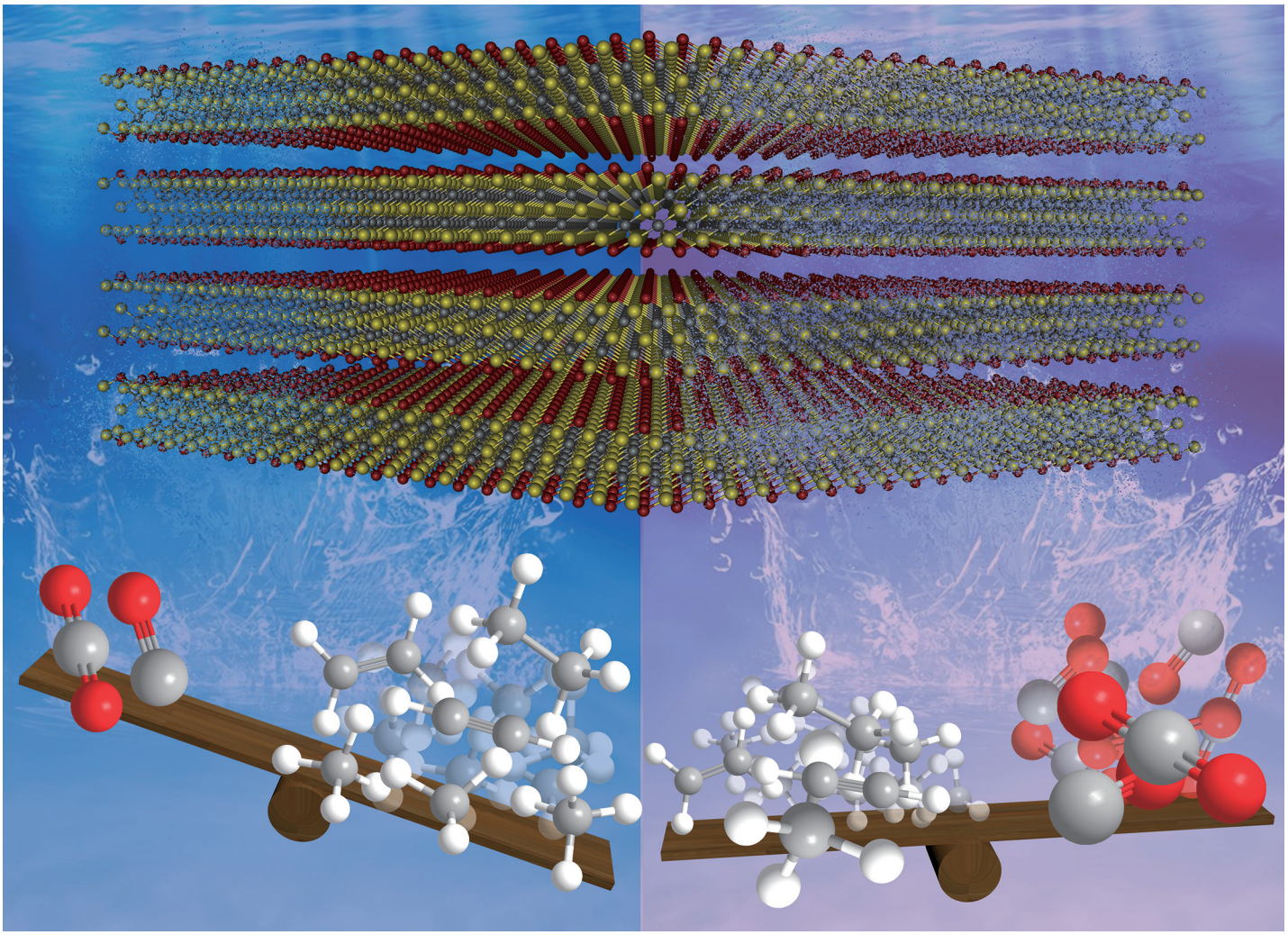

Showcasing collaborative research from Prof. Vadym Mochalin's laboratory, Department of Chemistry, Missouri University of Science and Technology, MO, USA and Prof. Shuohan Huang, College of Materials Science and Engineering, Donghua University, Shanghai, China.

Formation of hydrocarbons and carbon oxides in MXene reactions with water under varying oxidative conditions

We investigate reactions of 2D titanium carbide (MXenes) with water under varying oxidative conditions. Gas chromatography detected methane, carbon oxides, and, for the first time, C2 hydrocarbons. Methane dominates in low-oxidation environments (Ar-saturated water), while the concentration of carbon oxides increases with H_2O_2 addition. Formation of C2 hydrocarbons suggests radical recombination, challenging traditional carbide classifications and underscoring unique reactivity for application development.

Image reproduced by permission of Vadym N. Mochalin and Shuohan Huang from *Nanoscale*, 2025, **17**, 9937.

As featured in:

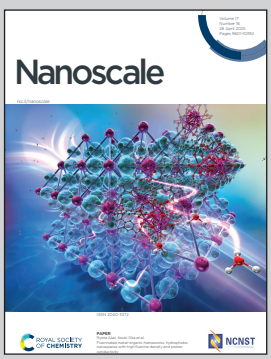

See Shuohan Huang, Vadym N. Mochalin *et al.*, *Nanoscale*, 2025, **17**, 9937.

ROYAL SOCIETY OF CHEMISTRY

rsc.li/nanoscale

Registered charity number: 207890

Nanoscale

ROYAL SOCIETY OF CHEMISTRY

PAPER

View Article Online
View Journal | View Issue

Cite this: *Nanoscale*, 2025, **17**, 9937

Formation of hydrocarbons and carbon oxides in MXene reactions with water under varying oxidative conditions†

Shuohan Huang, *[a] Guanglei Xiang[a] and Vadym N. Mochalin *[b,c]

Titanium carbide/carbonitride MXenes have garnered significant attention due to their remarkable properties, versatile solution processability, and broad range of potential applications. However, when exposed to the environment, MXenes are susceptible to degradation, which ultimately leads to the formation of metal oxides, a process that may be regarded as either disadvantageous or beneficial, depending on the application of a MXene and our knowledge about the underlying mechanisms. Therefore, it is very important to understand the reactivity of MXenes in different environments and conditions. Although researchers have made efforts to understand MXene degradation in air and water, our knowledge of the involved processes and even products of degradation remains incomplete. Here, we study the degradation of MXenes (Ti_2CT_x, $Ti_3C_2T_x$, and Ti_3CNT_x) under various oxidative conditions, in the presence of hydrogen peroxide, oxygen, ambient air, and argon. Gaseous products of MXene degradation in an aqueous environment were examined using gas chromatography (GC) equipped with a thermal conductivity detector (TCD) and a flame ionization detector (FID) working in series. In addition to methane and carbon dioxide, gaseous products including higher hydrocarbons were identified and analyzed. This research further deepens our understanding of the fundamental chemistry of MXenes.

Received 24th November 2024,
Accepted 18th February 2025

DOI: 10.1039/d4nr04937c

rsc.li/nanoscale

Introduction

Two-dimensional (2D) transition metal carbides and nitrides, known as MXenes, exhibit a very broad range of compositions compared to other 2D materials.[1] MXenes have the general formula $M_{n+1}X_nT_x$ (n = 1–4), where M represents an early transition metal, X can be carbon, nitrogen, or oxygen, and T denotes surface terminations such as –OH, –F, and –O–. Over the past decade following their discovery, MXenes have demonstrated an exceptional combination of physical and chemical properties, leading to a broad spectrum of potential applications including electromagnetic interference (EMI) shielding,[2,3] terahertz spectroscopy and communications,[4] wear reduction and lubrication,[5,6] energy storage,[7–9] molecular/ionic sieving,[10,11] sensors,[12–14] composites,[15,16] and many others.[17–19] However, since their discovery, MXenes have been known to be unstable, particularly in aqueous colloidal solutions, spontaneously transforming into the corresponding metal oxides over time, a process that usually results in loss of their functional properties,[20] but also provides opportunities to make new materials.[13,21–23]

Initial reports have been focused on studying and preventing oxidation as the main mechanism of MXene degradation. After the initial discovery of MXene hydrolysis[24] increasing attention has been directed toward understanding the chemical interactions between MXenes and water.[20,25,26] In our own subsequent work, analysis of the gaseous products was established as a sensitive and unambiguous technique to detect and monitor MXene degradation,[27] revealing that carbon and nitrogen of MXenes predominantly form CH_4 and NH_3, respectively. These experimental discoveries sparked the interest of theorists in using quantum chemical modeling to understand the underlying processes. Wu *et al.*[28] investigated the interaction between water molecules and the basal plane of the $Ti_3C_2O_2$ MXene using *ab initio* molecular dynamics (AIMD) simulations at room temperature (RT). Their findings revealed that the H_2O attack begins with the attachment (chemisorption) of a water molecule onto a Ti atom. This is followed by breaking Ti–C bonds and deprotonation of the water molecule, resulting in the formation of Ti–OH on the $Ti_3C_2O_2$ surface and the elimination of an H_3O^+ into the aqueous phase.

[a]*State Key Laboratory of Advanced Fiber Materials, College of Materials Science and Engineering, Donghua University, Shanghai 201620, China. E-mail: huangs@dhu.edu.cn*
[b]*Department of Chemistry, Missouri University of Science & Technology, Rolla, MO 65409, USA. E-mail: mochalinv@mst.edu*
[c]*Department of Materials Science & Engineering, Missouri University of Science & Technology, Rolla, MO 65409, USA*

† Electronic supplementary information (ESI) available. See DOI: https://doi.org/10.1039/d4nr04937c

Both chemical composition and surface functionalization significantly influence MXene stability. More recently, Song *et al.*[29] used AIMD to investigate the interaction between water and the defective $Ti_3C_2O_2$ MXene at RT. Their findings reveal that water molecules occupy the O vacancies and dissociate into OH groups and hydronium ions. The hydroxyl groups increase the negative charge on the MXene surface, which repels water O atoms, hindering their attachment to the Ti sites, thereby reducing the likelihood of further reactions. Additionally, they observed that a high concentration of –F groups on the MXene surface could prevent its degradation. Nesterova *et al.*[30] utilized enhanced sampling AIMD to study the role of terminating groups in the chemical stability of the $Ti_3C_2T_x$ MXene during its contact with water. Their findings showed that the reactivity of Ti towards water depends on the local coordination of Ti sites and the chemical composition of the MXene surface.

Despite these theoretical advancements, AIMD simulations are limited to extremely short time scales, typically picoseconds, meaning they can only capture the very first steps of MXene–water reactions. However, given that MXene degradation is likely a multistep process involving concurrent hydrolysis and oxidation reactions as well as ionic equilibria and polycondensations ultimately leading to transition metal oxides observed as the final products, the theoretical approaches alone cannot fully resolve the reaction mechanisms. This highlights the need for experimental studies to investigate the long-term evolution of MXenes under various environmental conditions. Experimental data not only provide direct evidence of reaction products but also serve as a critical input for refining computational models, ultimately improving our understanding of MXene reactivity.

Studies of the reactions of metal carbides with water have a long history, with metal carbides traditionally being divided into two main classes: those that readily react with water or dilute acids, and those that do not.[31,32] The carbides decomposable by water or aqueous mineral acids can be further subdivided into three groups: (a) forming methane during hydrolysis, like Fe_3C, Be_3C, and Al_4C_3; (b) forming acetylene upon hydrolysis, like the carbides of alkali, alkaline earth, and rare earth metals, where C≡C linkages exist in the crystal lattice (*e.g.*, CaC_2); and (c) forming propyne on hydrolysis, like Mg_2C_3, because of C–C≡C linkages present in its lattice.[32] Bulk TiC does not belong to any of these groups; it is inert towards water and is therefore traditionally classified, along with almost all other transition metal carbides, as non-reacting. This classification, although valid for bulk carbides, is being challenged when applied at the nanoscale to 2D forms of transition metal carbides, as we now know that titanium carbide MXenes spontaneously and completely react with water (hydrolysis) under ambient conditions (temperature, pH, and oxidizing strength), forming hydrocarbons and carbon oxides, thus showing dramatically different chemical properties compared to bulk TiC in the key reaction used for classification of carbides, *i.e.*, their hydrolysis.

In view of the above, careful identification of gaseous products of MXene hydrolysis and oxidation is important not only for a better understanding of MXene chemistry and ways to improve performance in applications, but it also may help us to clarify chemical properties and classification of metal carbides broadly defined. Our initial studies hypothesized about the evolution of CO, CO_2, CH_4, and H_2 during MXene hydrolysis, and experimentally confirmed the formation of CO_2 and CH_4.[24,27,33] Later, Doo *et al.*[34] detected the signals of CH_4, CO, CO_2, and HF during the degradation of the $Ti_3C_2T_x$ MXene in water using gas chromatography coupled with time-of-flight mass spectrometry. These results establish a firm basis for the idea that tracing the carbon containing products of MXene hydrolysis can provide valuable information about the fundamental mechanisms of MXene reactivity. To emphasize this idea, we mention parallels with a large body of research on products of bulk carbide hydrolysis. Initial studies of hydrolysis of Mn_3C carbide by Moissan revealed only CH_4 and H_2 as gaseous products, but later studies demonstrated that treatment of manganese carbide samples with hydrochloric acid solutions liberates only part of the carbide's carbon as volatile hydrocarbons, with free carbon and liquid hydrocarbons also being formed in the reaction.[35] It is not unlikely that MXene hydrolysis, in addition to already reported CH_4 and CO_2, may yield other products, albeit in smaller quantities. Moreover, the specific ratio of concentrations of different carbon containing products may depend on the nature of 2D carbide, properties of the environment, and conditions of the hydrolytic degradation, for example, oxidation strength and acidity of the environment, temperature, *etc.*

In this study, we investigated the volatile carbonaceous degradation products of 3 different titanium MXenes (Ti_2CT_x, Ti_3CNT_x, and $Ti_3C_2T_x$) exposed to various oxidation environments (aqueous H_2O_2, O_2, air, and Ar) using gas chromatography with a thermal conductivity detector (TCD) and a flame ionization detector (FID) working in series. The GC analysis of these products detected higher hydrocarbons in addition to methane, providing further important insights into the fundamental chemistry of 2D transition metal carbides and carbonitrides (MXenes).

Methods

Synthesis of MAX phases and MXenes

Ti_2AlC was synthesized by mixing TiC (2 μm size powder, 99.5%, Alfa Aesar), Ti (−325 mesh, 99.5%, Alfa Aesar), and Al (−325 mesh, 99.5%, Alfa Aesar) powders in a molar ratio of 0.85 : 1.15 : 1.05. To prevent the formation of transition metal binary carbides, the initial concentration of Al was adjusted to be slightly higher than the stoichiometric amount.[36] The mixture of dry powders was mechanically blended for 12 hours at RT, then heated at 10 °C min^{-1} to 1400 °C and held at this temperature for 4 hours under Ar flow. Ti_3AlC_2 was synthesized by mixing Ti, Al, and graphite powders (−325 mesh, 99%, Alfa Aesar) at a molar ratio of 3 : 1.1 : 1.88. This mixture was also blended for 12 hours and then heated at 10 °C min^{-1} to 1550 °C and held for 2 hours under Ar flow. Ti_3AlCN was syn-

thesized by mixing Ti, AlN (10 μm size powder, 98%, Sigma-Aldrich), and graphite powders at a molar ratio of 3 : 1.2 : 1. The mixture was blended for 12 hours at RT, heated at 10 °C min^{-1} to 1550 °C, and held at this temperature for 2 hours under Ar flow. The resulting MAX phase ceramic samples were manually crushed using a mortar and pestle.

The synthesis of Ti_2CT_x and $Ti_3C_2T_x$ MXenes followed previously described methods.[24,33] The as-synthesized MAX phase powder (Ti_2AlC or Ti_3AlC_2, 0.3 g, 325 mesh, particle size <38 μm) was gradually added to an etchant solution prepared by dissolving 0.6 g of LiF (97%, Alfa Aesar) in 6 ml of 9 M HCl (36 wt%, Alfa Aesar) in a loosely capped plastic 50 mL centrifuge tube. The mixture was stirred for 36 hours at 35 °C. For the synthesis of the Ti_3CNT_x MXene from the Ti_3AlCN MAX phase, 0.3 g of Ti_3AlCN powder (325 mesh, particle size <38 μm) was slowly added to an etchant solution prepared by dissolving 0.8 g of LiF in 10 ml of 9 M HCl in a 50 mL plastic centrifuge tube. The mixture was stirred for 18 hours at 40 °C. After etching, the mixtures were washed several times by repeated centrifugation and addition of fresh portions of deionized water until the pH of the supernatant reached approximately 6. Aqueous colloidal solutions of MXenes were obtained by mild ultrasonication at RT for 30 minutes in an ultrasonic bath (Bransonic M2800H) followed by centrifugation for 1 hour at 3500 rpm (Thermo Fisher Scientific Sorvall ST8 Centrifuge). The concentration of the freshly prepared MXene colloidal solutions was approximately 5 mg mL^{-1}.

Characterization of MAX phases and MXenes

X-ray diffraction (XRD) patterns of Ti_3AlC_2, Ti_3AlCN, and Ti_2AlC MAX phases, as well as $Ti_3C_2T_x$, Ti_3CNT_x, and Ti_2CT_x MXenes were obtained using a Bruker D8 Discover X-ray diffractometer (Diffrac Commander) with Cu K_α radiation (U = 40 kV and I = 40 mA). The measurements were recorded over a 2θ range from 5° to 85°.

UV–vis spectra of MXene colloidal solutions were measured in a quartz cuvette (1 cm path length) using a PerkinElmer Lambda 35 UV–vis spectrometer, covering a wavelength range of 400–850 nm.

Raman spectra of the MXenes were collected using a Renishaw InVia Raman microscope equipped with a 532 nm laser. Spectra were obtained with a 50× objective and a 1200 lines per mm grating, with an exposure time of 30 s, 1% laser power, and 10 accumulations.

Degradation of MXene samples under different environmental conditions

Four 6 mL aliquots of each MXene solution were transferred into separate 10 ml headspace vials. To the first vial, 100 μL of 30% H_2O_2 (Certified ACS, Thermo Fisher Scientific) was added. The remaining three vials were purged either with O_2 gas (UN1072 UHP, Airgas, 99.994%), ambient compressed air (laboratory-grade, moisture and CO_2-free, filtered) or Ar gas (UN1006 UHP300, Airgas, 99.999%), correspondingly, by bubbling the gas through the solution for 10 minutes (Fig. S1†). Immediately after purging, the vials were sealed, placed upside down to prevent gas escape through the cap, and stored at room temperature for approximately 1 day for the Ti_2CT_x MXene and approximately 5 days for Ti_3CNT_x and $Ti_3C_2T_x$ MXenes, before the aliquots of the gas phase were collected for analysis. For each environmental condition, the experiment was performed at least three times to ensure reproducibility of the results. The variability of gas composition measurements was within an acceptable range, with standard deviations provided in the ESI (Table S1†).

Analysis of gases formed during MXene degradation

Gas aliquots collected from the MXene samples in water under different atmospheres were analyzed using a Thermo Scientific Trace-1300 gas chromatograph. The instrument was equipped with a fused silica capillary column (Carboxen 1006 PLOT, 30 m length, 0.53 mm diameter, 30 μm thickness) coupled in series with TCDs and FIDs. Helium was used as both carrier and reference gas with flow rates of 4 and 4.3 mL min^{-1}, respectively. The parameters for the GC analysis were set as follows. For the first detector in series (TCD), the reference gas flow rate was 4.3 mL min^{-1}, the purge flow rate was maintained at 4 mL min^{-1}, and the TCD filament temperature was set to 280 °C. For the FID, the hydrogen gas, makeup gas (N_2), and airflow rates were 35, 40, and 350 mL min^{-1}, respectively, and the detector temperature was 250 °C. The column temperature was held at 50 °C for 4 minutes, then ramped up to 100 °C at a rate of 20 °C min^{-1} and held for 20 minutes. For each measurement, 0.1 mL of gas was manually injected into a GC injector using a 1 mL gastight syringe (Hamilton).

Computational modeling of MXenes and bulk carbides

Atomistic models of monolayer $Ti_2C(OH)_2$, $Ti_3C_2(OH)_2$, and $Ti_3CN(OH)_2$, as well as bulk CaC_2 were built and fully optimized using density functional theory (DFT) implemented in CASTEP.[37] Full geometry optimization with cell optimization was performed with the GGA PBE functional using ultrasoft pseudopotentials with Koelling–Hammon relativistic treatment with a plane-wave energy cut-off of 380 eV, 3 × 3 × 1 k points on a Monkhorst–Pack grid, and SCF tolerance of 5 × 10^{-7} eV per atom. Geometry was converged within 5 × 10^{-6} eV per atom energy, 0.01 eV A^{-1} force, 0.02 GPa stress, and 5 × 10^{-4} Å displacement. The parameters of the DFT optimized models are provided in Fig. S2.† These models were used to calculate the carbon–carbon pair distribution functions.

Results and discussion

Fabrication of MXene dispersions involves etching of aluminum from MAX phases, followed by delamination of multilayer MXenes in aqueous solutions. XRD analysis of Ti_3AlC_2, Ti_3AlCN, and Ti_2AlC MAX phases, along with their corresponding MXenes, confirms good quality of our MAX phases[2,24] and successful formation of MXenes, as evidenced by the shift of the (002) peak (Fig. 1a–c). UV–vis spectra show characteristic plasmon resonance peaks at ~758, 655, and 501 nm for

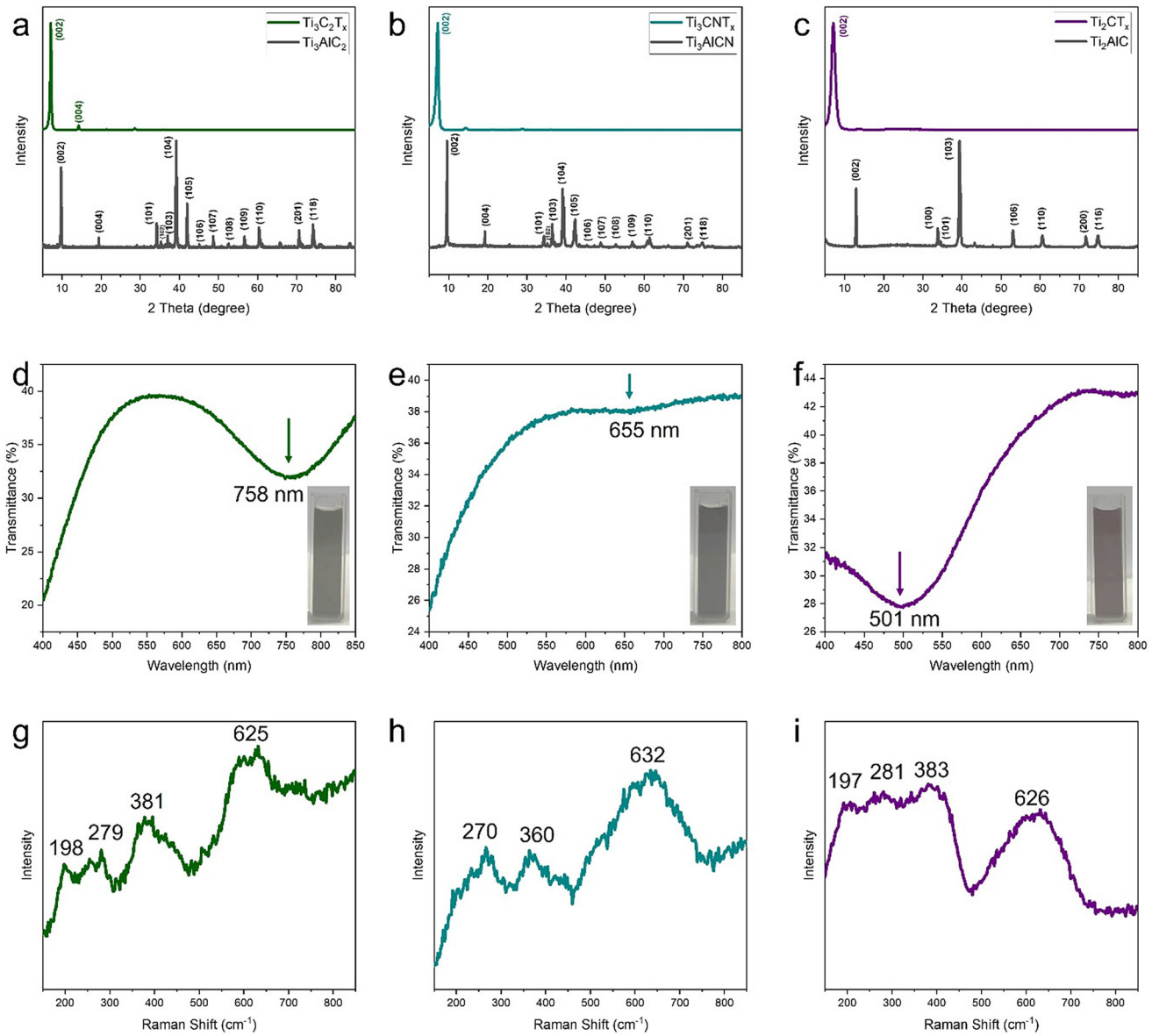

Fig. 1 (a–c) XRD patterns of Ti_3AlC_2, Ti_3AlCN, and Ti_2AlC MAX phases and their corresponding MXenes. (d–f) UV-vis spectra and (g–i) Raman spectra of $Ti_3C_2T_x$, Ti_3CNT_x, and Ti_2CT_x MXenes, respectively.

$Ti_3C_2T_x$, Ti_3CNT_x, and Ti_2CT_x dispersions, respectively (Fig. 1d–f).[38] Raman spectra of the MXenes (Fig. 1g–i), obtained after drying from freshly prepared colloidal solutions, show the expected vibration modes of MXenes, with patterns consistent with the reported literature for $Ti_3C_2T_x$, Ti_3CNT_x, and Ti_2CT_x MXenes.[24,39] The full-range Raman spectra in Fig. S3† show that the fresh MXenes do not exhibit any significant signals corresponding to sp^2 or amorphous carbon. Overall, the results of XRD, UV-vis, and Raman characterization confirm the successful synthesis of MXenes. Furthermore, the morphology of the tested samples was examined using AFM to show that all MXene samples were in a similar size range and had similar surface morphology (Fig. S4†).

An example of gas chromatography results (Fig. 2) shows the composition of the gaseous products from hydrolysis of the $Ti_3C_2T_x$ MXene in the presence of H_2O_2. On comparing the retention time of the detected compounds with the corresponding reference gases, we see signals of CO, CH_4, and CO_2 with the TCD, while the FID detected CO, CH_4, C_2H_2 (acetylene), C_2H_4 (ethylene), and C_2H_6 (ethane), identified by the coincidence of the retention time of the corresponding peaks with the retention time of the corresponding reference gases under the same conditions. The FID is much more sensitive to hydrocarbons than the TCD; therefore, it is not unusual that smaller concentrations of hydrocarbons can be seen with the FID while going undetected with the TCD. The green-colored area in the bottom panel, which is a zoomed-in view of the

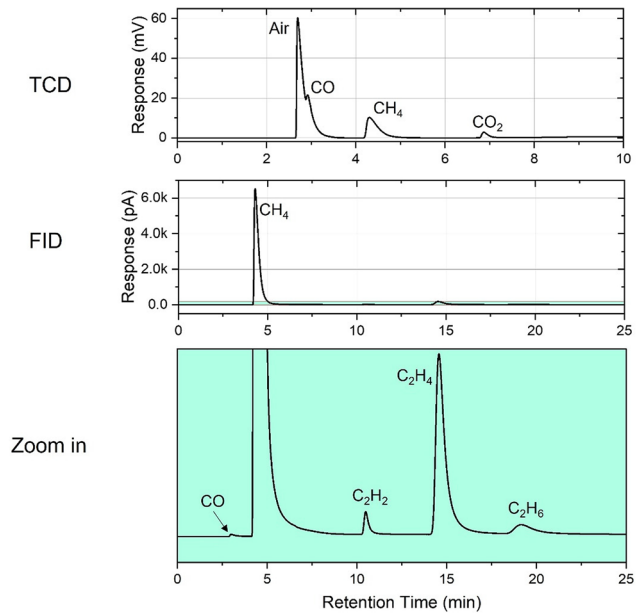

Fig. 2 Gas chromatographic analysis of gaseous products collected from hydrolysis of $Ti_3C_2T_x$ MXene in the presence of H_2O_2.

corresponding narrow area of the FID signal labeled in the middle panel, highlights the peaks of the three mentioned C2 hydrocarbons and a CO peak. We note that this is the first time when in addition to the previously detected gaseous products (CO, CO_2, and CH_4), C2 hydrocarbons were detected among the degradation products of MXenes.

Among metal carbides that react with water, LiC_2, CaC_2, SrC_2, and BaC_2 produce pure C_2H_2; Al_4C_3 and Be_2C produce pure CH_4; Mn_3C forms a mixture of H_2 and CH_4; and rare-earth carbides such as CeC, LaC, YC_2, and ThC_2 react with cold water forming a complex gas mixture containing H_2, C_2H_2, C_2H_4, and CH_4.[31] Based on the experimental results, titanium carbide MXenes exhibit properties similar to the above listed reactive metal carbides, rather than to their non-reacting bulk "cousin" TiC.

In the literature on bulk carbide hydrolysis, the formation of CH_4 is typically explained by the presence of methylene ($=CH_2$) radicals, which are primary products that undergo hydrogenation and/or polymerization to methane or hydrocarbon molecules with more carbon atoms.[32] For example, C_2H_6 is usually discussed as formed through the dimerization of $CH_3^{\bullet}$ radicals, which are present among hydrolysis products in small amounts. C_2H_2 is usually associated with preexisting C≡C linkages, and C_2H_4 with C=C linkages in the crystalline structure of carbides. However, as shown by radial distribution

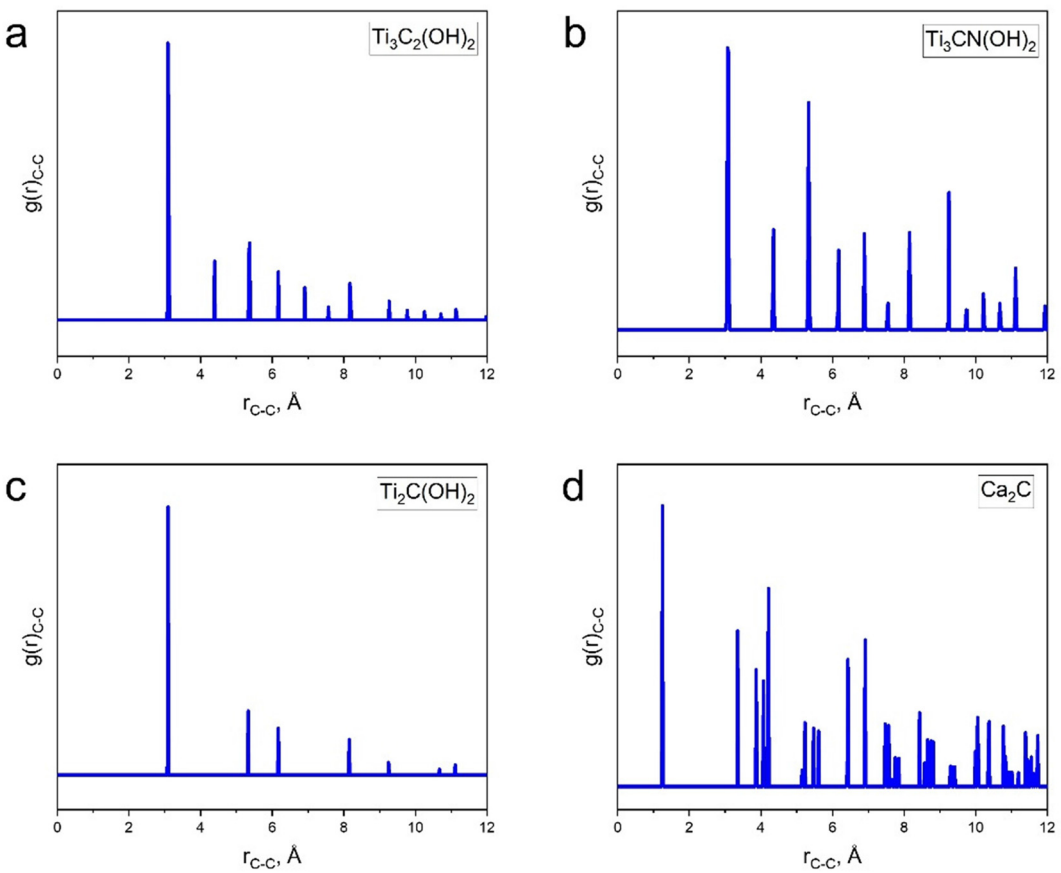

Fig. 3 C–C pair distribution functions calculated from atomistic models of (a) $Ti_3C_2(OH)_2$, (b) $Ti_3CN(OH)_2$, (c) $Ti_2C(OH)_2$ MXenes and (d) bulk CaC_2, which were optimized with density functional theory.

function analysis (Fig. 3), distances between any pair of carbon atoms in the MXene structure greatly exceed the C–C, C=C or C≡C bond length (fully OH terminated models were considered, but changing surface terminations from OH to O, F, or a mixture thereof does not change this conclusion). The shortest C–C distances measured with the optimized models are 3.089 Å for $Ti_3C_2(OH)_2$, 3.081 Å for $Ti_2C(OH)_2$, and 3.073–3.093 Å for $Ti_3CN(OH)_2$ in contrast to 1.253 Å for CaC_2. As expected, $Ti_3CN(OH)_2$ shows more disorder manifested by slightly broader peaks in its C–C radial distribution function (Fig. 3b); therefore, we list a range of shortest distances for this MXene.

Because there is no existing carbon–carbon linkages in the crystalline structure of these MXenes, the most plausible way to form C2 or higher hydrocarbons during MXene hydrolysis is through secondary post-hydrolytic reactions, *e.g.*, radical recombination, which is consistent with the low concentration of these larger molecules that we detected. Their low concentration explains why they were not detected before. Similar radical processes may be involved in the formation of free carbon during oxidative MXene degradation, as reported in some studies.[40–42] However, no solid carbon signals were detected in our experiments after the complete degradation of MXenes in water, leading to the conclusion that all MXene carbon atoms probably end up in molecular species.[27,43]

The formation of CO in hydrolysis of metal carbides is rarely reported. For instance, only 0.22% of CO was detected when Mn_3C was hydrolyzed by water at 20 °C.[35] CO and CO_2 are likely generated from the direct oxidation of MXene carbon by either H_2O or dissolved O_2. By considering MXene as an ionic crystal, the ionic nature of Ti_xC_y, *i.e.*, $Ti_x^{\frac{n}{x}+}C_y^{\frac{n}{y}-}$, suggests that electrons can be transferred from Ti atoms to C atoms within the MXene lattice. In the presence of the oxidizer, *e.g.* O_2, once the C atoms gain electrons from the Ti atoms, they become more prone to reducing water, leading to the formation of carbon oxides.[44]

Having identified the main and minor gaseous products, we further investigate their quantitative composition. A commercially available standard mixture of different gases was used to determine the gas composition. According to the manufacturer, this mixture included 1.00 mol% of C_2H_2, 1.00 mol% of CO_2, 1.00 mol% of CO, 1.02 mol% of C_2H_6, 1.00 mol% of C_2H_4, and 0.999 mol% of CH_4 (Scotty48, 48 Liters@300 psig, 21 °C, analyzed gases). When no strong oxidizers are present in the aqueous MXene colloidal solution, the

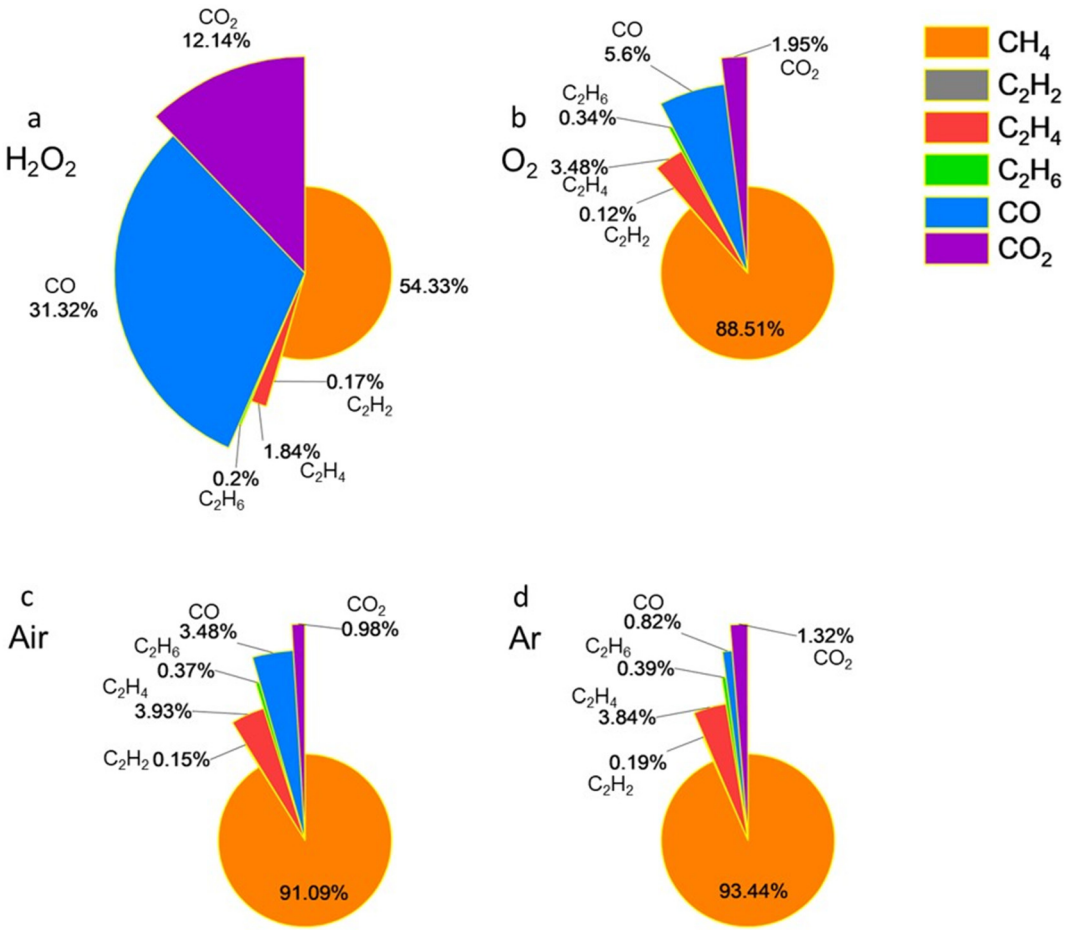

Fig. 4 Gaseous product composition of $Ti_3C_2T_x$ aqueous solution under the conditions of (a) H_2O_2, (b) O_2, (c) air, and (d) Ar.

majority of carbon atoms in $Ti_3C_2T_x$ convert into CH_4. As the oxidation potential of the environment increases, the formation of carbon oxides also increases. As shown in Fig. 4a, the addition of H_2O_2 to $Ti_3C_2T_x$ aqueous solution resulted in the production of 54.33 mol% CH_4, 2.21 mol% C2 hydrocarbons, and 43.46 mol% carbon oxides. For samples purged with and kept under an O_2 atmosphere, the measurements showed 88.51 mol% CH_4, 3.94 mol% C2 hydrocarbons, and 7.54 mol% carbon oxides (Fig. 4b). In the ambient air environment, the results were 91.09 mol% CH_4, 4.45 mol% C2 hydrocarbons, and 4.45 mol% carbon oxides (Fig. 4c). $Ti_3C_2T_x$ aqueous colloids purged with Ar gas produced 93.44 mol% CH_4, 4.42 mol% C2 hydrocarbons, and 2.14 mol% carbon oxides (Fig. 4d). Overall, as the environment became more reducing, the amount of CH_4 among the gas products increased, the amount of C2 hydrocarbons remained relatively constant and small, while the formation of carbon oxides decreased. This is consistent with hydrolysis becoming a more pronounced pathway of MXene degradation compared with oxidation under these conditions. Among the detected C2 hydrocarbons, C_2H_4 was consistently formed in greater quantities than C_2H_6 and C_2H_2, with their amounts remaining relatively similar. Therefore, the nature and content of hydrolysis products of MXenes in water depend on the oxidation potential of the environment.

As shown in Fig. 5a, the addition of H_2O_2 to Ti_3CNT_x aqueous colloidal solution resulted in the production of 33.38 mol% CH_4, 2.14 mol% C2 hydrocarbons, and 64.48 mol% carbon oxides. Under an O_2 atmosphere, the measurements gave 90.84 mol% CH_4, 3.37 mol% C2 hydrocarbons, and 5.79 mol% carbon oxides (Fig. 5b). In an air environment, the results were 95.32 mol% CH_4, 2.53 mol% C2 hydrocarbons, and 2.15 mol% carbon oxides (Fig. 5c). For Ti_3CNT_x samples purged with Ar gas, the analysis showed 96.75 mol% CH_4, 2.17 mol% C2 hydrocarbons, and 1.08 mol% CO_2 (well above ~0.04% naturally occurring in ambient air), with no CO detected (Fig. 5d).

For the Ti_3CNT_x MXene with the addition of H_2O_2, only approximately 33 mol% of CH_4 was formed, while more than 64 mol% of gaseous products were carbon oxides. As noted in our prior studies,[27] compared to $Ti_3C_2T_x$, random substitution of C atoms with N in Ti_3CNT_x increases the reactivity of the material, making it more susceptible to oxidation. Correspondingly, the composition of gases evolved from Ti_3CNT_x under O_2, air, and Ar atmospheres shows a typical ratio of products observed for other studied MXenes above, except that the percentage of CH_4 increased compared to $Ti_3C_2T_x$ in all three environments (O_2, air, and Ar), indicating an even higher reactivity of Ti_3CNT_x in hydrolysis compared to its oxidation, as CH_4 is a product of hydrolysis.

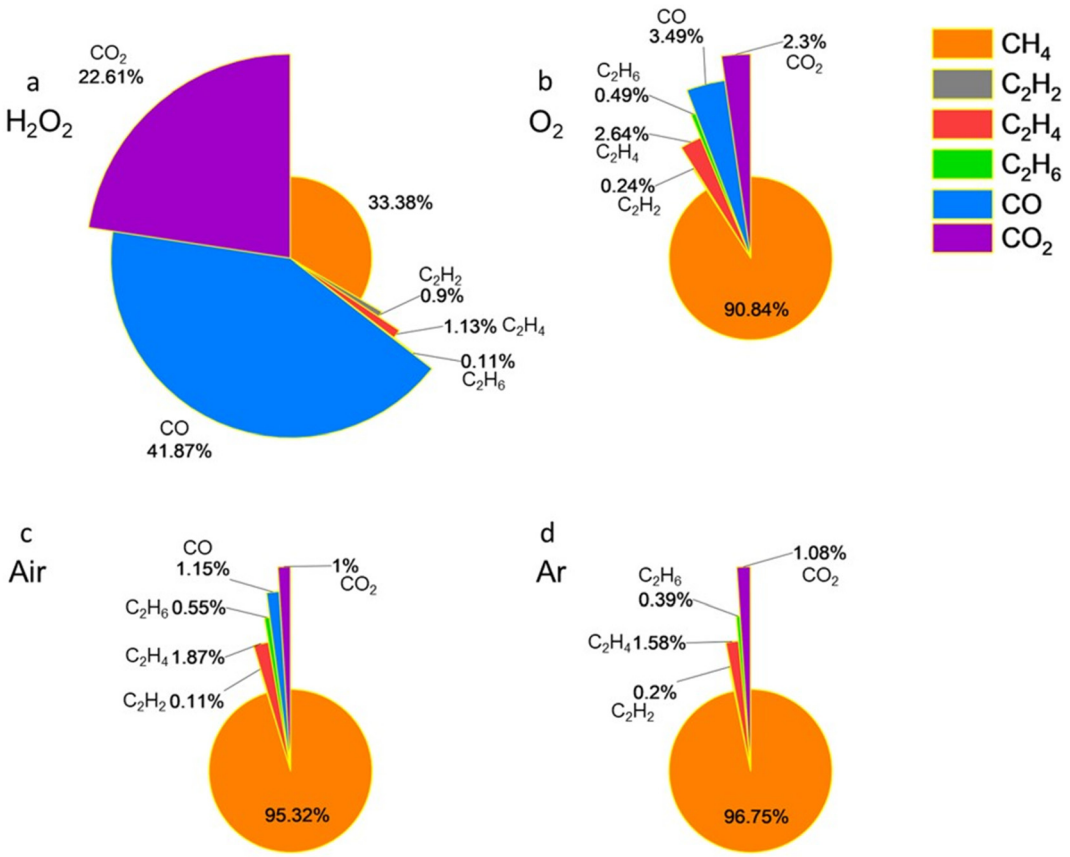

Fig. 5 Gaseous product composition of Ti_3CNT_x aqueous solution under the conditions of (a) H_2O_2, (b) O_2, (c) air, and (d) Ar.

The addition of H_2O_2 to the Ti_2CT_x aqueous solution (Fig. 6a) resulted in the production of 75.72 mol% CH_4, 5.41 mol% C2 hydrocarbons, and 18.87 mol% carbon oxides. Under an O_2 atmosphere, 97.86 mol% CH_4, 0.58 mol% C2 hydrocarbons, and 1.56 mol% CO_2 were formed (with no CO detected, Fig. 6b). In an air environment, the results were 98.94 mol% CH_4, 0.32 mol% C2 hydrocarbons, and 0.74 mol% CO_2 (with no CO detected, Fig. 6c). For Ti_2CT_x samples purged with Ar gas, GC analysis showed 99.48 mol% CH_4, 0.18 mol% C2 hydrocarbons, and 0.34 mol% CO_2 (with no CO detected, Fig. 6d). It is worth noting that trace amounts of C_2H_2, specifically 0.0012 mol%, 0.0004 mol%, and 0.0004 mol%, were still detectable among the degradation products of the Ti_2CT_x MXene in contact with O_2, air, and Ar atmospheres, respectively. But these amounts are insignificant and therefore we do not show them in Fig. 6b–d.

For Ti_2CT_x, more CH_4 was produced compared to the other MXenes. This might be explained assuming that higher hydrocarbons are formed in MXene hydrolysis *via* radical recombination processes, and since the Ti_2CT_x monolayer contains only one atomic layer of carbon whereas $Ti_3C_2T_x$ and Ti_3CNT_x both contain two, the likelihood of recombination of two radicals formed in the process of stepwise C–Ti bonds breaking during Ti_2CT_x degradation is significantly lower compared to other studied MXenes with a thicker monolayer that provides a higher local concentration of C atoms and therefore higher likelihood of radical recombination. When the probability for recombination is low, it is more likely that all carbon atoms will eventually saturate their unsaturated valences by a stepwise process of binding hydrogen from water and forming CH_4, as observed for Ti_2CT_x.

Interestingly, small but measurable quantities of H_2 were detected among degradation products of Ti_2CT_x in aqueous colloids under both air and Ar atmospheres (Fig. 7). We never observed H_2 formation with other MXenes and it is not quite clear how it can be formed. One hypothetical source of H_2 might be H^+, which was evidenced in MXene degradation by a drop in pH of solutions over time from freshly made until their complete degradation.[27] These protons in solution could in turn originate either from not completely removed HF species or from the reactions of functional groups (at least some of the T_x contain hydrogen atoms, *e.g.*, OH), or they could be protons formed by the attack of H_2O on MXenes, when OH groups of water are attached to Ti atoms forming Ti $(OH)_n$ (n = 1–4) and hydrogen atoms can either attach to C atoms in MXenes forming hydrocarbons or, if there are not enough C atoms, will form protons that can be solvated by water and reduced to H_2 later. In the latter case, when there are not enough C atoms for the reaction with all H atoms from the attacking water molecules, one cannot exclude recombination of H atoms from water with the direct formation of H_2. It is not clear at present which of these processes (if any) results

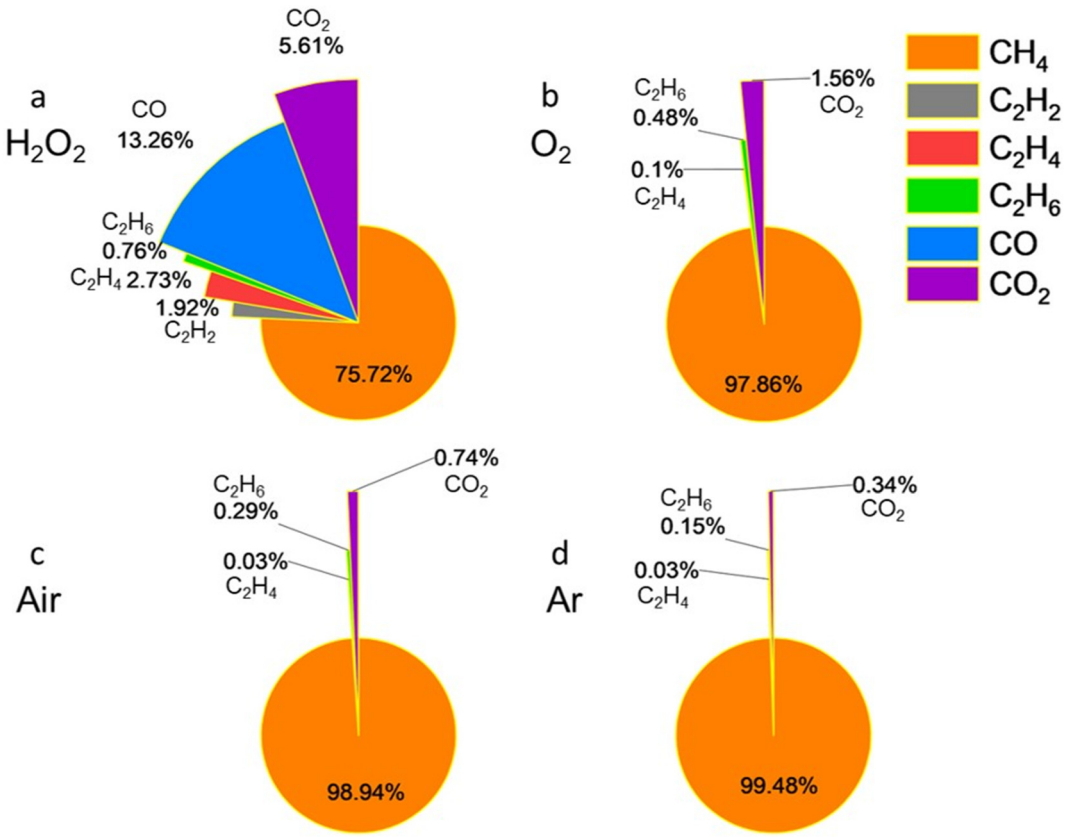

Fig. 6 Gaseous product composition of Ti_2CT_x aqueous solution under the conditions of (a) H_2O_2, (b) O_2, (c) air, and (d) Ar.

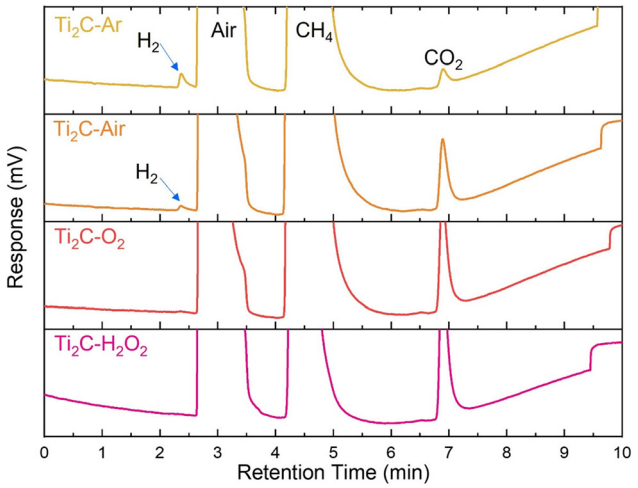

Fig. 7 GC-TCD analysis of gaseous products from the hydrolysis of the Ti_2CT_x MXene in different environments.

in the detected H_2, but it is noted that we only detect H_2 signal from Ti_2CT_x samples under air and, to a larger extent, under Ar atmospheres, *i.e.*, when the oxidation strength of the environment is relatively low, which agrees with the abovementioned hypotheses.

While the detection of C2 hydrocarbons among the products of MXene hydrolysis is interesting, we note that even more complex products have been observed in hydrolysis of some of the bulk carbides in the past. For example, bulk uranium carbide, U_2C_3, when reacted with water yields significant amount of liquid and solid hydrocarbons in addition to a gaseous mixture containing methane, ethylene, and hydrogen.[31,45] Similarly, more complex products, including higher hydrocarbons, may also be anticipated in hydrolysis of MXenes, especially of those MXenes which have not been studied yet and thus, warrant further investigation in future research.

Conclusions

In conclusion, this study explores the degradation behavior of titanium containing MXenes (Ti_2CT_x, $Ti_3C_2T_x$, and Ti_3CNT_x) in water across various oxidation environments, including hydrogen peroxide, oxygen, air, and argon. Gas chromatography analysis revealed the formation of gaseous products such as methane, carbon oxides, and, for the first time, C2 hydrocarbons (ethylene, acetylene, and ethane), broadening our understanding of MXene chemistry. According to our results, methane is the dominant product under reducing conditions, while the production of carbon oxides increases in the environments with higher oxidation potential. This research offers insights into the hydrolysis and oxidative degradation mechanisms of MXenes, in comparison with bulk metal carbides, thereby challenging our traditional knowledge of carbide chemistry. We believe that this information will also contribute to a more rational development of various applications of MXenes.

Author contributions

Shuohan Huang: writing – original draft, methodology, data curation, conceptualization, and funding acquisition; Guanglei Xiang: formal analysis, writing – review and editing, and validation; Vadym N. Mochalin: writing – review and editing, conceptualization, supervision, and funding acquisition.

Data availability

The data supporting this article have been included as part of the ESI.†

Conflicts of interest

The authors declare that they have no known competing financial interests or personal relationships that could have appeared to influence the work reported in this paper.

Acknowledgements

This work was supported by the Fundamental Research Funds for the Central Universities (2232022D-03) and the National Natural Science Foundation of China (No. 52402102). We acknowledge funding support for this research from the National Science Foundation (DMREF-2324156).

References

1 M. Naguib, V. N. Mochalin, M. W. Barsoum and Y. Gogotsi, *Adv. Mater.*, 2014, **26**, 992–1005.
2 A. Iqbal, F. Shahzad, K. Hantanasirisakul, M.-K. Kim, J. Kwon, J. Hong, H. Kim, D. Kim, Y. Gogotsi and C. M. Koo, *Science*, 2020, **369**, 446–450.
3 C. Liu, Y. Ma, Y. Xie, J. Zou, H. Wu, S. Peng, W. Qian, D. He, X. Zhang, B.-W. Li and C.-W. Nan, *ACS Appl. Mater. Interfaces*, 2023, **15**, 4516–4526.
4 G. Li, N. Amer, H. A. Hafez, S. Huang, D. Turchinovich, V. N. Mochalin, F. A. Hegmann and L. V. Titova, *Nano Lett.*, 2020, **20**, 636–643.
5 S. Huang, K. C. Mutyala, A. V. Sumant and V. N. Mochalin, *Mater. Today Adv.*, 2021, **9**, 100133.
6 A. Rosenkranz, M. C. Righi, A. V. Sumant, B. Anasori and V. N. Mochalin, *Adv. Mater.*, 2023, **35**, 2207757.
7 J. Yang, M. Li, S. Fang, Y. Wang, H. He, C. Wang, Z. Zhang, B. Yuan, L. Jiang, R. H. Baughman and Q. Cheng, *Science*, 2024, **383**, 771–777.

8 M. Lai, C. Zhao, D. Wang, R. Gao, P. Cai, L. Sun, Q. He, H. Peng, H. Zhang, F. Xu, C. Hu, K. Liang and C. J. Zhang, *ACS Appl. Mater. Interfaces*, 2024, **16**, 55555–55568.
9 W. Zhang, C. Zeng, M. Zhang, C. Zhao, D. Chao, G. Zhou and C. Zhang, *Angew. Chem., Int. Ed.*, 2025, **64**, e202413728.
10 X. Zhu, M. Lou, J. Chen, X. Fang, S. Huang and F. Li, *Appl. Surf. Sci.*, 2023, **625**, 157194.
11 Y. Li, X. Zhu, Q. Gao, Y. Bai, M. Lou, S. Huang, F. Li and B. Van der Bruggen, *J. Membr. Sci.*, 2024, **712**, 123236.
12 H. Zhang, Y. He, Y. Xia, Y. Chen, Y. Wang, R. Weng, T. Zhang and S. Huang, *Mater. Today Chem.*, 2024, **38**, 102088.
13 S. Chertopalov and V. N. Mochalin, *ACS Nano*, 2018, **12**, 6109–6116.
14 Q. He, C. Zhao, H. Chen, T. Wu, C. Zeng, Y. Chen and C. Zhang, *J. Mater. Chem. A*, 2024, **12**, 25622–25642.
15 L. Bi, W. Perry, R. Wang, R. Lord, T. Hryhorchuk, A. Inman, O. Gogotsi, V. Balitskiy, V. Zahorodna, I. Baginskiy, S. Vorotilo and Y. Gogotsi, *Adv. Funct. Mater.*, 2023, **34**, 2312434.
16 A. Baimenov, C. Daulbayev, S. G. Poulopoulos and V. N. Mochalin, *Mater. Today*, 2024, **78**, 75–91.
17 S. Abdolhosseinzadeh, R. Schneider, M. Jafarpour, C. Merlet, F. Nüesch, C. Zhang and J. Heier, *Adv. Electron. Mater.*, 2025, **11**, 2400170.
18 T. Guo, D. Zhou, S. Deng, M. Jafarpour, J. Avaro, A. Neels, J. Heier and C. Zhang, *ACS Nano*, 2023, **17**, 3737–3749.
19 T. Guo, D. Zhou, M. Gao, S. Deng, M. Jafarpour, J. Avaro, A. Neels, E. Hack, J. Wang, J. Heier and C. Zhang, *Adv. Funct. Mater.*, 2023, **33**, 2213183.
20 K. P. Marquez, K. M. D. Sisican, R. P. Ibabao, R. A. J. Malenab, M. A. N. Judicpa, L. Henderson, J. Zhang, K. A. S. Usman and J. M. Razal, *Small Sci.*, 2024, **4**, 2400150.
21 P. Ridley, C. Gallano, R. Andris, C. E. Shuck, Y. Gogotsi and E. Pomerantseva, *ACS Appl. Energy Mater.*, 2020, **3**, 10892–10901.
22 M. A. K. Purbayanto, M. Chandel, D. Bury, A. Wójcik, D. Moszczyńska, A. Tabassum, V. N. Mochalin, M. Naguib and A. M. Jastrzębska, *Langmuir*, 2024, **40**, 21547–21558.
23 M. A. K. Purbayanto, D. Bury, M. Chandel, Z. D. Shahrak, V. N. Mochalin, A. Wójcik, D. Moszczyńska, A. Wojciechowska, A. Tabassum, M. Naguib and A. M. Jastrzębska, *ACS Appl. Mater. Interfaces*, 2023, **15**, 44075–44086.
24 S. Huang and V. N. Mochalin, *Inorg. Chem.*, 2019, **58**, 1958–1966.
25 F. Cao, Y. Zhang, H. Wang, K. Khan, A. K. Tareen, W. Qian, H. Zhang and H. Ågren, *Adv. Mater.*, 2022, **34**, 2107554.
26 R. A. Soomro, P. Zhang, B. Fan, Y. Wei and B. Xu, *Nanomicro Lett.*, 2023, **15**, 108.
27 S. Huang and V. N. Mochalin, *ACS Nano*, 2020, **14**, 10251–10257.
28 T. Wu, P. R. C. Kent, Y. Gogotsi and D.-e. Jiang, *Chem. Mater.*, 2022, **34**, 4975–4982.
29 H. Song and D.-e. Jiang, *Nanoscale*, 2023, **15**, 16010–16015.
30 V. Nesterova, V. Korostelev and K. Klyukin, *J. Phys. Chem. Lett.*, 2024, **15**, 3698–3704.
31 G. N. H, *Nature*, 1896, **54**, 357–357.
32 G. L. Putnam and K. A. Kobe, *Chem. Rev.*, 1937, **20**, 131–143.
33 S. Huang, V. Natu, J. Tao, Y. Xia, V. N. Mochalin and M. W. Barsoum, *J. Mater. Chem. A*, 2022, **10**, 22016–22024.
34 S. Doo, A. Chae, D. Kim, T. Oh, T. Y. Ko, S. J. Kim, D.-Y. Koh and C. M. Koo, *ACS Appl. Mater. Interfaces*, 2021, **13**, 22855–22865.
35 W. R. Myers and W. Fishel, *J. Am. Chem. Soc.*, 1945, **67**, 1962–1964.
36 M. N. Abdelmalak, *MXenes: A new family of two-dimensional materials and its application as electrodes for Li-ion batteries*, Drexel University, 2014.
37 S. J. Clark, M. D. Segall, C. J. Pickard, P. J. Hasnip, M. I. J. Probert, K. Refson and M. C. Payne, *Z. Kristallogr. – Cryst. Mater.*, 2005, **220**, 567–570.
38 K. Shevchuk, A. Sarycheva and Y. Gogotsi, *MRS Bull.*, 2022, **47**, 545–554.
39 S. Huang and V. N. Mochalin, *Inorg. Chem.*, 2022, **61**, 9877–9887.
40 H. Ghassemi, W. Harlow, O. Mashtalir, M. Beidaghi, M. Lukatskaya, Y. Gogotsi and M. L. Taheri, *J. Mater. Chem. A*, 2014, **2**, 14339–14343.
41 M. Naguib, O. Mashtalir, M. R. Lukatskaya, B. Dyatkin, C. Zhang, V. Presser, Y. Gogotsi and M. W. Barsoum, *Chem. Commun.*, 2014, **50**, 7420–7423.
42 Y. Liu, Z. Shi, T. Liang, D. Zheng, Z. Yang, Z. Wang, J. Zhou and S. Wang, *InfoMat*, 2024, **6**, e12536.
43 B. Ahmed, D. H. Anjum, M. N. Hedhili, Y. Gogotsi and H. N. Alshareef, *Nanoscale*, 2016, **8**, 7580–7587.
44 Y. Hori and T. Mukaibo, *Bull. Chem. Soc. Jpn.*, 1968, **41**, 1983–1989.
45 S. El Jamal, M. Johnsson and M. Jonsson, *ACS Omega*, 2021, **6**, 24289–24295.